Thermal conductivity of condensed gold in states with the strongly excited electron subsystem

2015 J. Phys.: Conf. Ser. 653 012087

(http://iopscience.iop.org/1742-6596/653/1/012087)

Thermal conductivity of condensed gold in states with the strongly excited electron subsystem

Yu V Petrov[1,2], N A Inogamov[1], S I Anisimov[1], K P Migdal[3], V A Khokhlov[1] and K V Khishchenko[4,2]

[1] Landau Institute for Theoretical Physics of the Russian Academy of Scienses, Akademika Semenova 1a, Chernogolovka, Moscow Region 142432, Russia
[2] Moscow Institute of Physics and Technology, Institutskiy Pereulok 9, Dolgoprudny, Moscow Region 141700, Russia
[3] All-Russia Scientific Research Institute of Automatics, Sushchevskaya 22, Moscow 127055, Russia
[4] Joint Institute for High Temperatures of the Russian Academy of Sciences, Izhorskaya 13 Bldg 2, Moscow 125412, Russia

E-mail: nailinogamov@googlemail.com

Abstract. Data on thermal conductivity in states with hot electrons are necessary for the calculation of ultrashort laser exposure and the behavior of matter near the tracks of fast particles penetrating the condensed phase. The paper presents new analytical expressions describing the state of gold with the extra-high heat conductivity within a broad range of two-temperature phase diagram including the melting curve. This is a region in the three-dimensional space defined by the electron temperature T_e, ion temperature T_i and the density ρ, at which the thermal conductivity κ is one order of magnitude larger than the value related to the room temperature. The growth of heat transfer is due to a sharp increase in the heat capacity of carriers (electrons) when they are heated and, accordingly, the gradual loss of the degeneracy. The developed model is based on an exact solution of the kinetic equation, involving experimental data and calculations of the electronic spectrum by the density functional method. The model works well also at low temperatures T_e that allows describing the crystallization of the melt as it cools down.

1. Introduction

Analysis of the problems of radiation physics requires knowledge of the transport characteristics of substances in the two-temperature (2T) states [1–7]. Another important set of applications is associated with ultrashort laser exposure [8–16]. In typical laser applications [9, 11, 14–22], ablation of substance is studied, when a matter response has two-temperature (2T) stage with electron and ion temperatures $T_e \sim$ 10–30 kK, $T_i \sim$ 0.3–10 kK and densities of the order of a solid-state density. An example of temperature and density instantaneous profiles under the heating by the laser radiation is shown in figure 1.

In the example, 2T stage is still quite far from completeness; the electron temperature is much higher than the ion temperature. The instant $t = 5$ ps is shown. The calculation parameters are as follows: the absorbed fluence is $F_{\rm abs} = 130$ mJ/cm^2, a gold target occupies a half-space, pulse duration is $\tau_L = 70$ fs, the skin layer has a 15 nm thickness, a Lagrangian coordinate step is 1 nm. A system of 2T hydrodynamics equations, equation of state and other parameters

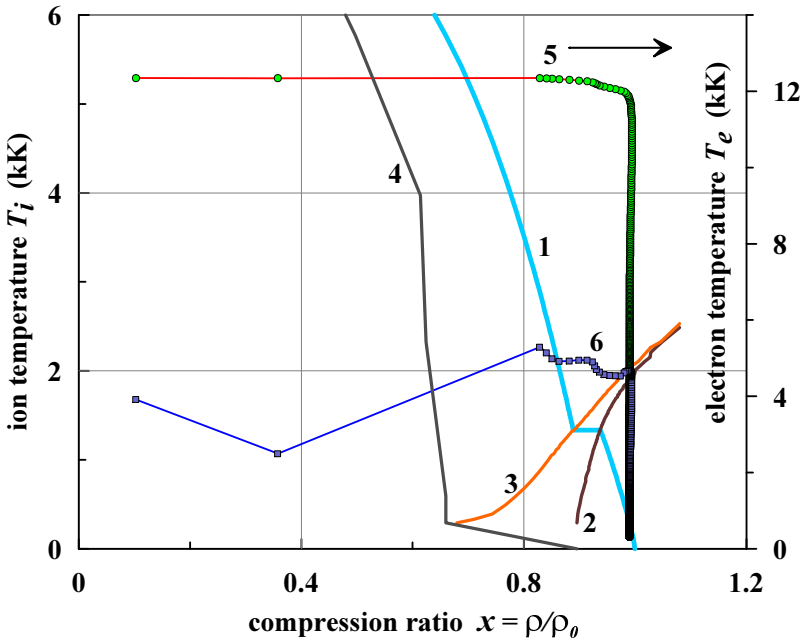

Figure 1. Curves 1–4 represent the binodal, solidus, liquidus and spinodal of gold according to a multiphase equation of state [23, 24], referring to the plane ρ–T_i. Electron T_e and ion T_i temperatures at the instant 5 ps are shown by the curves 5 and 6, corresponding respectively to the right and left vertical axes. Thus, all curves belong to the left axis, and the only curve 5 showing the electron temperature distribution belongs to the right axis. This is emphasized by the arrow near the digit "5".

used can be found elsewhere [22]. 2T hydrodynamic code, written in Lagrangian variables, is used. Figure 1 allows us to estimate the size of three-dimensional domain T_e, T_i, ρ, where these parameters are located. It follows from figure 1, that the deviation from the isochore on 2T stage is associated with the rarefaction wave into the vacuum.

2T equation of state is based on the free energy potential F presented as the sum of electron F_e and ion F_i contributions: $F(T_e, T_i, \rho) = F_i(T_i, \rho) + F_e(T_e, \rho)$, where the ion contribution $F_i = F_c(\rho) + F_t(T_i, \rho)$ is the sum of cold and heat contributions [22–28]. Thus, in a 2T situation *two* thermal contributions—electron $F_e(T_e, \rho)$ and ion $F_t(T_i, \rho)$ are added to the cold energy F_c. At zero temperature $T_e = T_i = 0$, the expressions for the free energy and the internal energy are identical, so we can talk about the cold energy.

Sharp turn of curves 5 and 6 from the vertical direction to the horizontal direction is associated with the decreasing of density in the rarefaction wave propagating with the speed of sound from the vacuum boundary. Parent rarefaction wave characteristic is located at the 17 nm depth at the instant 5 ps (penetration depth is measured from the initial position of the vacuum boundary). Electron thermal wave moving at 2T stage at supersonic speed penetrates deep into the semi-infinite target of gold. The point, at which the temperature T_e is equal to half-maximum instantaneous temperature at the instant 5 ps, is at 160 nm depth. Far from the surface temperature T_e and T_i are equal to the room temperature 300 K.

Markers as circles and squares on the curves 5 and 6 show the positions of the points of uniform Lagrangian coordinate differences. The last two points are detached from the main mass of Lagrangian points. They correspond to the tail of the rarefaction wave, which is the vapor [29]. Due to the large values of the electron pressure, at an early 2T stage a "cold" evaporation takes place, i.e. evaporation at high electron temperatures T_e, but low ion temperature T_i. Analysis

of cold evaporation is done in works [15, 30].

From a series of calculations with $F_{\text{abs}} = 130$ mJ/cm^2 executed with different steps on the Lagrangian coordinates, it follows that, at the instant 5 ps, the mass of gold in the evaporated tail is equal to the mass in a layer of 1.6 nm thickness at the equilibrium density 19.3 g/cm^3. For comparison, at the one-temperature $T = T_e = T_i$ vacuum evaporation of gold, heated to a temperature $T = 2$ kK (as in figure 1), 3–4 orders of magnitude smaller mass is evaporated during 5 ps.

As it can be seen, the equation of state, the electron–ion heat transfer and thermal conductivity (heat wave spread) questions are important for a quantitative description of the action of femtosecond laser pulses. A new analytical model of heat conduction is presented in the description below.

2. Scheme of decomposition into components in the 2T model of thermal conductivity

The importance of the problem of describing the transport characteristics is well recognized, starting with the work [8]. Theoretical models [9, 12, 13, 31, 32] depart from the Matthiessen rule (composition of resistivities) and the Drude formulas for the electrical conductivity $\sigma = n_e e^2/(m_e \nu)$, and thermal conductivity $\kappa = c_e v^2/(3\nu)$ with the electron collision frequency in the form of $\nu = AT_i + BT_e^2$.

Coefficient A in the frequency ν_{ei} of electron–ion collisions is taken from the resistivity of solid metal, and the electron–electron coefficient B in the frequency ν_{ee} is determined by the order of magnitude $\nu_{ee} \sim (E_{\text{F}}/\hbar)(k_{\text{B}}T_e/E_{\text{F}})^2$. Here σ, n_e, e, m_e, κ, c_e and v are the conductivity, density, charge and mass of the electron, electronic thermal conductivity, electronic heat capacity per unit volume and the average velocity of the electrons, respectively. Moreover, the electron–electron contribution to ν_{ee} dominates at high electron temperatures.

Our model has the following peculiarities. First of all, it is a neat calculation of electron–electron interactions using the kinetic theory [12, 26]. In doing this, it is taken into account the presence of d-band in noble and transition metals. The calculations show that the collision frequency ν_{ee} at $T_e \sim 1$ eV and higher is significantly below than that one given by a rough estimate of $\nu_{ee} \sim (E_{\text{F}}/\hbar)(k_{\text{B}}T_e/E_{\text{F}})^2$. Also, we take into account the jump in the resistance and density at the melting. The experimental data are taken adjusted for the fact that they were obtained on the binodal (curve 1 in figure 1) where the density decreases with increasing temperature (thermal expansion). The results are presented in an analytical form suitable for the use in 2T codes.

3. Electron–electron contribution

Matthiessen rule on the thermal conductivity κ_{se}, due to the scattering of electrons on the s-electrons is given by $1/\kappa_{se} = 1/\kappa_{ss} + 1/\kappa_{sd}$, where contributions of s–s and s–d collisions are presented. At s–d collisions, s-electron interacts with the electrons of the d-band. In principle, there is a channel of heat conductivity through the d-electrons. Then, according to the rule of composition of parallel channels the total thermal conductivity is equal to $\kappa_{se} + \kappa_{de}$. The calculations show that the contribution of κ_{de} is negligible. In figure 2, circles show the results of calculations of thermal conductivity κ_{se} by solving the kinetic equation by the method of [12,26].

The calculations are performed with the Thomas–Fermi screening for the two-parabolic model of the electron spectrum [12, 26]. Parameters of parabolic bands $E_s = -9.2$ eV, $E_1 = -6.8$ eV, $E_2 = -1.7$ eV are found by using the density functional theory in the package VASP [33]. Here E_s, E_1 and E_2 are the bottom of the s-band, the bottom of the d-band and the top of the d-band respectively, measured from the Fermi level. The solid curve in figure 2 gives an analytic

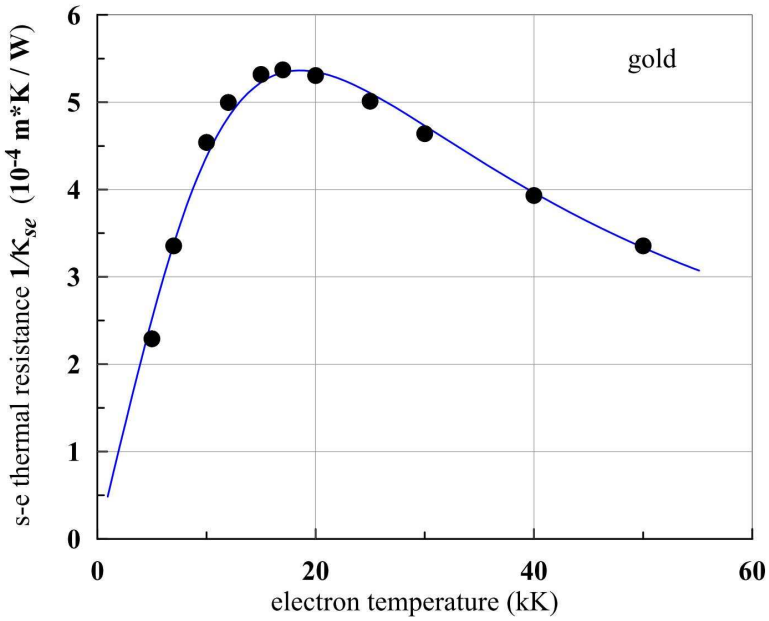

Figure 2. The dependence of the electron–electron thermal resistivity $1/\kappa_{se}$ on the electron temperature T_e at normal density $x = 1$, $\rho = \rho_0$. The continuous curve is calculated by formula (1), circles mark solutions of kinetic equations. Analytical dependence (1) has the asymptotic behavior of $\kappa_{se} \propto 1/T_e$ at low temperatures and $\kappa_{se} \propto T_e$ at $k_\mathrm{B}T_e \sim E_\mathrm{F}$.

approximation expressed in m K/W,

$$\frac{1}{\kappa_{se}(T_e, x)} = \frac{10^4\, x^{-4/3}\, a_0\, t}{1 + b_0\sqrt{t} + b_1\, t + b_2\, t^2}, \tag{1}$$

where $a_0 = 9.294$, $b_0 = 0.03$, $b_1 = -0.2688$, $b_2 = 0.9722$. We neglect the dependence of $\kappa_{se}(T_e, x)$ on the ion temperature T_i, since in noble metals it is weak [26,34,35]. At a fixed number density of ions, electronic spectrum rather weakly depends on the phase (solid or liquid) of the metal. Therefore, we use the approximation (1) in solid and liquid phases alike. In the expression (1) the normalized temperature $t = 6k_\mathrm{B}T_e/E_\mathrm{F} = 6k_\mathrm{B}T_e/(xE_{\mathrm{F}0})$, where k_B—the Boltzmann constant, is used. From our calculations [28], it follows that, in the case of gold, at the variation of compression ratio $x = \rho/\rho_0$ Fermi energy is proportional to the first degree of x: $E_\mathrm{F} = xE_{\mathrm{F}0}$; and it is not proportional to $x^{2/3}$; here $E_{\mathrm{F}0}$ is the Fermi energy at $x = 1$. Band structure calculations [28], showing that $E_\mathrm{F} \propto x$, are carried out using the package VASP [33].

4. Electron–ion contribution in the solid phase

Let us consider the contribution to the conductivity σ and thermal conductivity κ, associated with the electron–phonon interaction in the solid phase:

$$\sigma_{si} = n_e e^2 \lambda_{si}/p_\mathrm{F}, \quad \kappa_{si} = c_e v \lambda_{si}/3. \tag{2}$$

We assume that the mean free path length λ_{si} is the same in expressions (2) for σ and κ. In (2), n_e, e, p_F, c_e, v and $\lambda_{si} = 1/(n\Sigma_{si})$ are respectively number density of conduction electrons, the electron charge, the Fermi momentum $p_\mathrm{F} = \hbar(3\pi^2 n_e)^{1/3}$, electronic heat capacity per unit volume, average speed and the mean free path, due to scattering by phonons. In addition,

$$\Sigma_{si} \sim u_0^2(T_i/\theta), \quad u_0 \sim \hbar/\sqrt{Mk_\mathrm{B}\theta}, \tag{3}$$

where Σ_{si} is the effective cross section of the electron–phonon interaction and u_0 is the amplitude of zero-point vibrations of the atom with mass M; n is the atom number density, $\theta \propto c_S n^{1/3}$ is the Debye temperature, c_S is the sound velocity, $k_\mathrm{D} = (6\pi^2\, n)^{1/3}$ is the Debye wave number. From the expressions (3), it follows that

$$\lambda_{si} \propto \theta^2/(nT_i). \tag{4}$$

Thus, when calculating the mean free path (4) and transport characteristics the dependence of the Debye temperature θ on the dimensionless density x, defined above becomes important. The fact is that the dependence of the elastic constants and hence the sound velocity on the density is important. Indeed, the variation of density changes force that returns the atom into the equilibrium position as it vibrates in the crystalline lattice: potential well holding the atom becomes wider with a density decrease. Accordingly, the oscillation amplitude, the square of which defines a cross section of electron–phonon scattering, is changed. Moreover, the speed of sound and the slope of the potential well are strongly dependent on the density variation, as spinodal (where $c_T = 0$) is close to the binodal at the phase diagram. Namely, the minimum of cold curve on the spinodal (see below) is achieved by only 25% stretching with respect to the equilibrium density.

5. Variation of the density and the Debye temperature

To describe analytically the effect of tension and compression, we need a cold-pressure dependence upon the density. We represent it as the sum of the attractive (b) and repulsive ($a > b$) parts:

$$p_c = An_0x(x^a - x^b), \tag{5}$$

where n_0 is the number density of atoms in equilibrium at $T = 0$, $p = 0$. Parameters in the expression (5) $A = 14.6$ eV/atom, $a = 3.92$, $b = 1.95$ are defined to reproduce reference value of the bulk modulus of gold $K = 220$ GPa under normal conditions, cohesive energy 3.78 eV/atom [36] and the reference value 14.2×10^{-6} K^{-1} of the thermal expansion coefficient under normal conditions [37]. For these values of the parameters (A, a, b), minimal pressure on the cold curve (5) is equal to $p_\mathrm{min} = -26.0$ GPa. Pressure p_min is achieved by expanding to $x_\mathrm{min} = 0.77$. Coordinates of the pressure minimum are consistent with the commonly used data ($x_\mathrm{min} = 0.74$, $p_\mathrm{min} = -21$ GPa) [38, 39].

With binomial formula (5) for cold pressure p_c, the expression for the Debye temperature has the form

$$\theta(x) = \frac{\hbar}{k_\mathrm{B}} c_{S1} k_\mathrm{D1} x^{1/3} \sqrt{y(x)}, \tag{6}$$

$$y(x) = [(a+1)x^a - (b+1)x^b]/(a-b),$$

where $y \propto K = \rho \mathrm{d}p_c/\mathrm{d}\rho$, K is the bulk modulus.

In relation (6), the speed of sound $c_{S1} = c_S(x = 1)$ averaged over directions by using the relation $3/c_S^3 = 1/c_l^3 + 2/c_t^3$ and Debye wave number $k_\mathrm{D1} = k_\mathrm{D}(x = 1)$ are taken at the equilibrium density $x = \rho/\rho_0 = 1$, where $\rho_0 = 19.5$ g/cm^3—equilibrium density of gold for $p = 0$, $T = 0$; c_l and c_t are longitudinal and transverse sound velocity in the isotropic solid model

$$c_l = \sqrt{[(1-\sigma_\mathrm{P})/(1+\sigma_\mathrm{P})]3K/\rho},$$

$$c_t = \sqrt{[(1/2)(1-2\sigma_\mathrm{P})/(1+\sigma_\mathrm{P})]3K/\rho},$$

here σ_P is the Poisson ratio.

Later in the analytical formulas, we will use the function

$$\bar{y}(x) = (1 + c_{ab})\, x^\alpha/(1 + c_{ab}\, x^\beta), \tag{7}$$

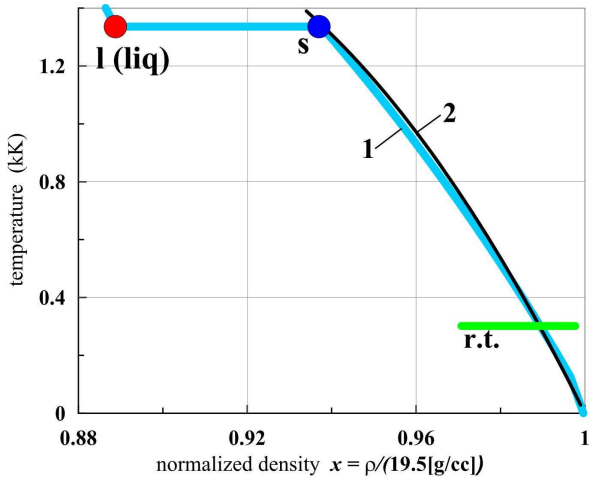

Figure 3. Comparison of approximation (8) (curve 2) with the binodal (curve 1) taken from figure 1. Markers "s" and "l" are the ends of the triple point segment from the solid and liquid phases respectively. To the left of point "l" binodal (curve 1) is called the boiling curve.

$$\alpha = 2a + 1, \quad \beta = a + 1, \quad c_{ab} = (a - b)/(b + 1),$$

instead of the function $y(x)$. The fact is that the function $y \propto K = x\,\mathrm{d}p_c/\mathrm{d}x$ vanishes at the minimum of cold pressure (5) that is the point of intersection of the spinodal and $T = 0$ axis. At lower relative densities x function $y(x)$ becomes negative, and the Debye temperature (6) and the speed of sound become imaginary. It does not make it possible to perform a through numerical simulation at low densities that arise in the rarefaction wave and at the substance spallation. The mass of layers of low density is small; they do not play a significant role in the energy balance. In addition, our model does not claim to provide for an accurate description of the thermal conductivity at very low densities. In our problems, it is important to present accurate kinetic characteristics at moderate (tens of percent) density variations around the equilibrium value. Parameters of the function $\bar{y}(x)$ (7) are chosen so that the functions $\bar{y}(x)$ and $y(x)$ are close to each other near the equilibrium density $x = 1$. As it can be seen, the function $\bar{y}(x)$ (7) is positive at $x \to 0$.

In experimental data references [37,40,42], electrical conductivity σ and thermal conductivity κ are given at the binodal 1 in figure 1 as in stationary conditions the tested wire expands when heated. Let us see how well the binomial expression (5) approximates the curve of sublimation, the lower segment of the binodal, referring to the solid state, see figures 1 and 3. To do this, we calculate the Grüneisen parameter $G(x) = \mathrm{d}\ln\theta/\mathrm{d}\ln x$ with the value of θ (6). We write the Mie–Grüneisen equation of state [43]. As a result, we find the equation of zero-pressure isobar:

$$p_c(n) + 3G(n)nk_\mathrm{B}T_i = 0 \tag{8}$$

or $A(x^a - x^b) + 3G(x)k_\mathrm{B}T = 0$, if we use binomial expression for p_c (5). Zero isobars equation $p(\rho, T) = 0$ coincides with the curve of sublimation, if we neglect the insignificant vapor pressure (below the triple point pressure of the vapor is much less than pressures ~ 1 GPa, interesting for us in connection with the laser applications.

Figure 3 shows a comparison of the approximation of sublimation curve (8) obtained by the use of expression (5) for cold pressure with the sublimation curve from the wide-range equation of state [23, 24]. As we can see, there is a good agreement of the two curves. In figure 3, sublimation curve from [23,24] is a segment between the points $x = 1$, $T = 0$ and "s"; horizontal line "r.t." corresponds to a temperature 300 K.

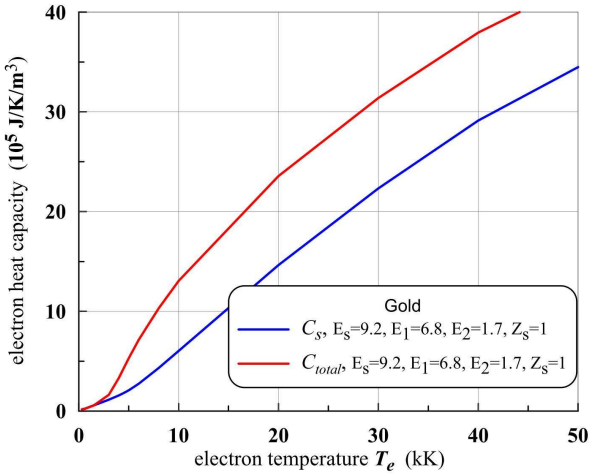

Figure 4. Comparison of total (s + d), and partial (s) electronic heat capacity. Heat capacities c_s and c_total are calculated by using the two-parabolic approximation of the electron spectrum with the parameters specified in the sidebar. Here $E_\mathrm{s} = E_{\mathrm{F}0}$ is a bottom of the s-band, measured from the Fermi level, E_1 and E_2 are edges of the d-band. The calculation is performed at $x = 1$.

6. Conductivity and thermal conductivity of the crystalline gold

As mentioned, our goal is to obtain analytical expressions for the transport coefficients of gold in two-temperature (2T) states. Moreover, these expressions must describe 2T, as well as the one-temperature (1T: at $T_e = T_i = T$) states, because hydrodynamic code describes the current situation from 2T stage with hot electrons and 1T stage of melt cooling and recrystallization. The desired expression for the thermal resistance in the solid phase has the form

$$1/\kappa_\mathrm{sol} = 1/\kappa_{se} + 1/\kappa_{si}^\mathrm{sol}. \tag{9}$$

In the expression (9), electron–electron contribution to the thermal conductivity κ_{se} is given by equation (1). As mentioned in section 3, the contribution of d-electrons in the heat transfer is small. Therefore, in the expression (9) electron–electron contribution is indicated by the index se, which means the s-electron scattering on the s- and d-electrons.

Coefficient of thermal conductivity due to electron–ion collisions in a solid (solid state is indicated by the top index "sol") phase κ_{si}^sol in the expression (9) is calculated by the formula

$$\kappa_{si}^\mathrm{sol} = (1/3) n k_\mathrm{B} C(t) v_\mathrm{F} \lambda_{si}, \tag{10}$$

ascending to expression (2). In formula (10), a dimensionless factor $C(t)$, where $t = 6k_\mathrm{B}T_e/(xE_{\mathrm{F}0})$, is selected, which comprises the dependence of heat capacity and average speed of s-electrons upon the electron temperature T_e (and x). The heat capacity of the s-electrons is calculated in the framework of the two-parabolic approximation of the electron spectrum [12] and significantly differs from the total electron heat capacity of gold, see figure 4.

For an average speed of s-electrons, we take the value of $v = v_\mathrm{F}\sqrt{1 + 3k_\mathrm{B}T_e/(2xE_{\mathrm{F}0})}$. Fermi velocity $v_\mathrm{F} = p_\mathrm{F}/m_*$ depends on the number density through the Fermi momentum $p_\mathrm{F} \propto n^{1/3}$ and the effective mass m_*, which at $E_\mathrm{F} \propto n$ satisfies the condition $m_* \propto n^{-1/3}$, so

$$v_\mathrm{F} = v_{\mathrm{F}0}\, x^{2/3}, \tag{11}$$

where $v_{\mathrm{F}0}$ is the Fermi velocity at $x = 1$. The mean free path of electrons at s–scattering by phonons in the solid phase λ_{si} is expressed in terms of the Debye temperature by formula

(4). Debye temperature θ can be represented as an expression close to (6), but we replace the function $y(x)$ with the function $\bar{y}(x)$ (7), which does not change the sign for expansions outside the spinodal. As a result, we obtain

$$\theta^2(x) = \theta^2(1)\, x^{2/3}\, \bar{y}(x).$$

Accordingly, for the electron mean free path at the electron–phonon scattering we obtain

$$\lambda_{si} \propto \bar{y}(x) x^{-1/3} T_i^{-1}. \tag{12}$$

We introduce the value

$$\kappa_0(t) = (1/3) n_0^{2/3} k_{\rm B} C(t) v_{\rm F0},$$

having the thermal conductivity dimension. Then, from the above formulas (10), (11) and (12) we obtain

$$\kappa_{si}^{\rm sol} \propto \kappa_0(t)\, x^{4/3} \bar{y}(x) T_i^{-1}.$$

The function $\kappa_0(t)$ was calculated for crystalline gold at $x = 1$. The resulting dependence of the normalized electron temperature t can be approximated by

$$\kappa_0(t) = 131\, t\, (1 + 3.07\, t^2)/(1 + 1.08\, t^{2.07}),$$

κ_0 is given in W/(m K). We denote $x_{rt} = 19.3/19.5$ relative density of gold on the sublimation curve at room $T_{rt} = 0.293$ kK temperature. Considering also that the experimental value of the thermal conductivity under these conditions is equal to 318 W/(m K), we obtain the coefficient of the electron thermal conductivity in units of W/(m K) when electron–phonon scattering in the solid phase

$$\kappa_{si}^{\rm sol}(T_e, T_i, x) = 318 \left(\frac{x}{x_{rt}}\right)^{4/3} \frac{\bar{y}(x)}{\bar{y}(x_{rt})} \frac{T_{rt}}{T_i} \frac{\kappa_0(t)}{\kappa_0(t_{rt})}, \tag{13}$$

where $t_{rt} = 6 k_{\rm B} T_{rt}/(x_{rt} E_{\rm F0})$.

In a similar manner an expression for the resistivity of $r = 1/\sigma$ of solid gold is derived. Rewrite (2) by using formula (4). As a result, we obtain

$$r = [(3\pi^2)^{1/3}/(2\pi)] R_0 n^{2/3}/\lambda_{si} \propto x^{1/3} T_i/\theta^2,$$

where $R_0 = h/e^2 = 25812.8\ \Omega$ is a quantum of electrical resistance. Taking into account the formula for the Debye temperature (6), in which the function $y(x)$ is replaced by $\bar{y}(x)$, we have

$$r(T_i, x) = r_{rt} \frac{T_i}{T_{rt}} \left(\frac{x_{rt}}{x}\right)^{1/3} \frac{\bar{y}(x_{rt})}{\bar{y}(x)}, \tag{14}$$

where $r_{rt} = 22.14$ nΩ m is a gold resistivity at room temperature.

Figure 5 shows the resistivity behavior obtained by the use of formula (14), together with the experimental data [42]. The dashed curve shows the temperature dependence of the resistivity $r(T, x_{rt})$ for the isochore $\rho = 19.3$ g/cm^3. The solid curve corresponds to the dependence of the resistivity upon temperature along the curve of sublimation, it takes into account the effect of thermal expansion of gold. Sublimation curve is given by the expression $x_{\rm bin} = 0.852 + 0.105\sqrt{1.98 - T}$. As one can see, the calculated values for the binodal are in a good agreement with the data [42]. Comparison of resistivity for isochore and binodal (sublimation curve) shows that the thermal expansion makes a governing contribution to the difference between the solid and dashed curves.

Figure 6 indicates the dependence of thermal conductivity (13) on the temperature. Here calculations at the relative density isochore x_{rt} (dashed curve) and the binodal (solid curve) are presented. The dots show the experimental data taken from handbooks [37, 40].

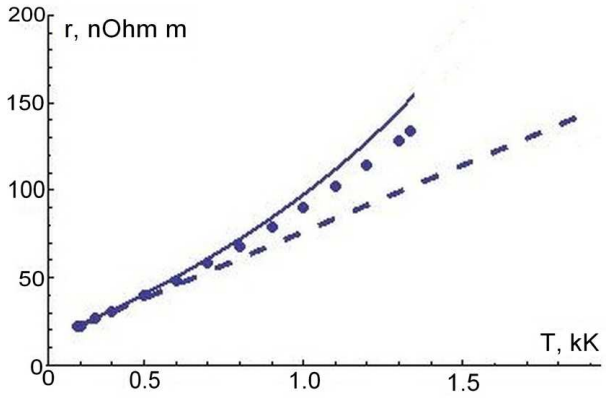

Figure 5. The resistivity of gold in the solid state depending on temperature in the equilibrium one-temperature case. The solid curve—resistivity at the sublimation binodal, dashed curve—at isochore 19.3 g/cm^3, both calculated according to formula (14). Also experimental data [42] (full circles) are shown.

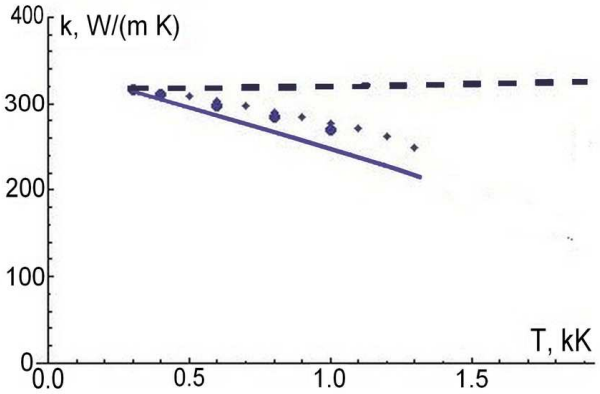

Figure 6. Comparison of thermal conductivity on the binodal (solid curve) and normal density isochore (dashed curve) with the experimental data (large circles—[37], small points—[40]). The thermal conductivity was calculated according to formula (13).

7. Electron–ion contribution in the liquid phase

We calculate the thermal conductivity of 2T molten gold. Electron–electron contribution is still given by (1). We need to write the approximation expression for the contribution of the electron–ion scattering. Assuming that in the liquid phase electron mean free path λ_l due to the electron–ion scattering can be written, as in the solid phase, in factorized form $\lambda_l = n_0^{-1/3} W(T_i) x^\beta$, and again using the value $\kappa_0(T_e, x)$, we have for the coefficient of thermal conductivity

$$\kappa_{ei}^{\mathrm{liq}}(T_e, T_i, x) = \kappa_0(T_e, x)\, x\, x^{2/3} W(T_i) x^\beta.$$

Drude formula for resistivity gives

$$r(T_i, x) = \frac{p_\mathrm{F}}{n e^2 \lambda_l} = \frac{(3\pi^2)^{1/3}}{2\pi} R_0 \frac{n_0^{1/3}}{n^{2/3} W(T_i) x^\beta} = \frac{r_0}{x^{2/3} W(T_i) x^\beta}.$$

Here $r_0 = (3\pi^2)^{1/3} R_0/(2\pi) n_0^{-1/3} = 3254$ nΩ m. Designating $\gamma = \beta + 2/3$, we have

$$r(T_i, x) = \frac{r_0}{W(T_i) x^\gamma}.$$

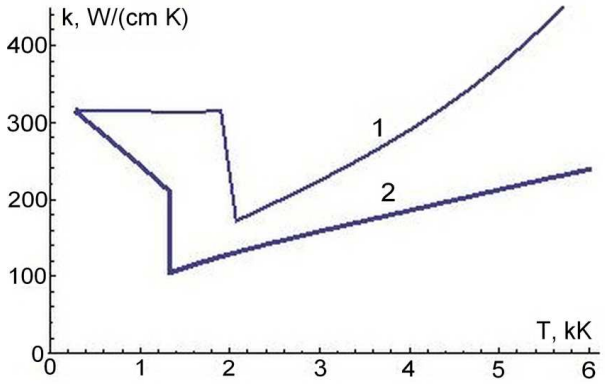

Figure 7. Electron thermal conductivity coefficient of gold as a function of the temperature T, the same for ions and electrons: 1—on the isochore of 19.3 g/cm^3; 2—on the binodal curve consisting of sublimation and boiling curve.

According to quantum molecular dynamics calculations [41] we take $\gamma = 2$. Function $W(T)$ can be found by the use of known experimental dependence $r_l(T)$ of the resistivity of gold upon the temperature along the boiling curve $x_l(T)$ [37], so that

$$W(T) = \frac{r_0}{r_l(T)x_l^{\gamma}(T)}.$$

Boiling curve for the temperature T in kK is given as

$$x_l(T) = 0.887179 - 0.0328321(T - 1.337) - 0.0030982(T - 1.337)^2 - 0.000164884(T - 1.337)^3$$

with a resistivity in the units of nΩ m on it

$$r_l(T) = 148.5 + 119.3T15.337/(14 + T),$$

which coincides with the known experimental data and tends to the minimum metallic conductivity in strongly disordered ion system at high ion temperatures.

Then we obtain the coefficient of thermal conductivity in the liquid phase due to electron–ion collisions in the form

$$\kappa_{ei}^{\mathrm{liq}}(T_e, T_i, x) = \kappa_0(T_e, x)\frac{r_0}{r_l(T_i)}x\left(\frac{x}{x_l(T_i)}\right)^{\gamma}.$$

The total thermal conductivity coefficient in liquid phase is given with taking into account κ_{se}, so that the heat resistivity is

$$1/\kappa_{\mathrm{liq}} = 1/\kappa_{se} + 1/\kappa_{ei}^{\mathrm{liq}}. \tag{15}$$

Figure 7 shows the electron thermal conductivity of gold depending on the temperature for one-temperature situation in the state of thermal equilibrium between electrons and ions on the binodal curve covering the sublimation and boiling curve, as well as on the normal density isochore. Phase transition leads to a jump in the thermal conductivity on the binodal and slightly more smooth transition from its value in the solid phase to the value of the melt on isochore.

Electronic thermal conductivity in two-temperature situation, characteristic for the interaction of ultrashort laser pulses with metals, as a function of the electron temperature for several values of the ion temperature in both the solid and liquid phases is shown in figure 8. The nonmonotonic behavior of the coefficient of thermal conductivity in the solid phase at

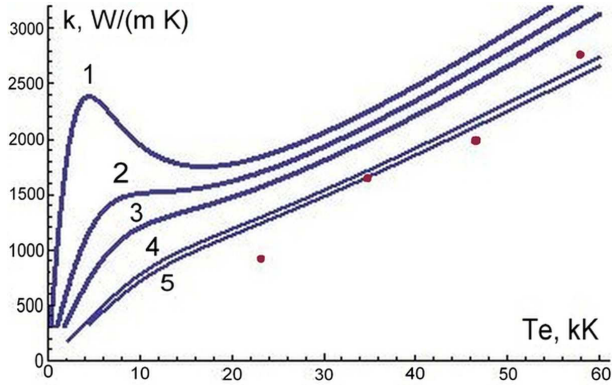

Figure 8. Electron thermal conductivity coefficient of gold as a function of the electron temperature T_e in the 2T-case. Curves 1, 2, 3 refer to the solid phase (1—at ion temperature $T_i = 0.293$ kK, 2—$T_i = 1$ kK, 3—$T_i = 1.8$ kK), curves 4 and 5 refer to the liquid phase (4—$T_i = 2.2$ kK, 5—$T_i = 4.5$ kK). Relative density $x = x_{rt} = 19.3/19.5$. Red points show results obtained by the quantum molecular dynamics in [44] for the case $x = 19.3/19.5$, $T_i = 300$ K.

relatively low ion temperatures is due to significantly weaker increase of the electron–electron collisions as the electron temperature increases above 10 kK than at lower temperatures of the electrons, whereas the continuing increase of the heat capacity of s-electrons and their average velocity takes place.

8. Conclusion

Electron thermal conductivity coefficient of gold depending on the electron and ion temperatures and density is obtained in the analytical form suitable for use in two-temperature hydrodynamic and molecular dynamics codes. Both the electron–ion and electron–electron scattering are taken into account [12, 26] in the metal with s- and d-electrons. The analytical expressions allow calculating the coefficient of electron thermal conductivity in a wide range of electron and ion temperatures as well as densities, which is of interest in the problems of laser ablation of metals as in the solid phase as in the melt, taking into account the jump at the phase transition.

Acknowledgments

The work is partially supported by the Russian Foundation for Basic Research grants No. 13-02-01078 (Y V P, N A I, S I A, K P M, V A K), 13-02-91057 (K V K) and 13-08-12248 (K V K).

References

[1] Kaganov M I, Lifshitz I M and Tanatarov L V 1957 *Sov. Phys. JETP* **4** 173
[2] Dremov V V, Karavaev A V, Sapozhnikov F A, Vorobyova M A, Preston D L and Zocher M A 2011 *J. Nucl. Mater.* **414** 471
[3] Povarnitsyn M E, Andreev N E, Levashov P R, Khishchenko K V and Rosmej O N 2012 *Phys. Plasmas* **19** 023110
[4] Povarnitsyn M E, Andreev N E, Levashov P R, Khishchenko K V, Kim D A, Novikov V G and Rosmej O N 2013 *Laser Part. Beams* **31** 663
[5] Norman G E, Starikov S V, Stegailov V V, Zhilyaev P A and Saitov I M 2013 *Contrib. Plasma Phys.* **53** 129
[6] Charakhch'yan A A and Khishchenko K V 2015 *Laser Part. Beams* **33** 65
[7] Andreev N E, Povarnitsyn M E, Veysman M E, Faenov A Ya, Levashov P R, Khishchenko K V, Pikuz T A, Magunov A I, Rosmej O N, Blazevic A, Pelka A, Schaumann G, Schollmeier M and Roth M 2015 *Laser Part. Beams* **33** 541
[8] Anisimov S I, Kapeliovich B L and Perelman T L 1974 *Sov. Phys. JETP* **39** 375

[9] Furusawa K, Takahashi K, Kumagai H, Midorikawa K and Obara M 1999 *Appl. Phys.* A **69** [Suppl.] S359
[10] Povarnitsyn M E, Itina T E, Sentis M, Khishchenko K V and Levashov P R 2007 *Phys. Rev.* B **75** 235414
[11] Povarnitsyn M E, Itina T E, Levashov P R and Khishchenko K V 2013 *Phys. Chem. Chem. Phys.* **15** 3108
[12] Petrov Yu V, Inogamov N A and Migdal K P 2013 *JETP Lett.* **97** 20
[13] Knyazev D V and Levashov P R 2014 *Phys. Plasmas* **21** 073302
[14] Emel'yanov V I, Danilov P A, Zayarnyi D A, Ionin A A, Kudryashov S I, Makarov S V, Rudenko A A, Shikunov D I and Yurovskikh V I 2014 *JETP Lett.* **100** 145
[15] Inogamov N A, Zhakhovsky V V, Khokhlov V A, Ashitkov S I, Emirov Yu N, Khichshenko K V, Faenov A Ya, Pikuz T A, Ishino M, Kando M, Hasegawa N, Nishikino M, Komarov P S, Demaske B J, Agranat M B, Anisimov S I, Kawachi T and Oleynik I I 2014 *J. Phys.: Conf. Series* **510** 012041
[16] Povarnitsyn M E, Fokin V B and Levashov P R 2015 *Appl. Surf. Sci.* **357** 1150
[17] Gill-Comeau M and Lewis L J 2011 *Phys. Rev.* B **84** 224110
[18] Bezhanov S G, Kanavin A P and Uryupin S A 2011 *Quantum Electron.* **41** 447
[19] Loboda P A, Smirnov N A, Shadrin A A and Karlykhanov N G 2011 *High Energ. Dens. Phys.* **7** 361
[20] Povarnitsyn M E, Knyazev D V and Levashov P R 2012 *Contrib. Plasma Phys.* **52** 145
[21] Wu Ch and Zhigilei L V 2014 *Appl. Phys.* A **114** 11
[22] Inogamov N A, Zhakhovsky V V and Khokhlov V A 2015 *JETP* **120** 15
[23] Khishchenko K V 2008 *J. Phys.: Conf. Series* **98** 032023
[24] Khishchenko K V 2008 *J. Phys.: Conf. Series* **121** 022025
[25] Bushman A V, Kanel' G I, Ni A L and Fortov V E 1993 *Intense Dynamic Loading of Condensed Matter* (London: Taylor Francis)
[26] Migdal K P, Petrov Yu V and Inogamov N A 2013 *Proc. SPIE* **9065** 906503
[27] Khishchenko K V 2015 *J. Phys.: Conf. Series* This issue (*Preprint* `arXiv:1510.00763`)
[28] Petrov Yu V, Migdal K P, Inogamov N A and Zhakhovsky V V 2015 *Appl. Phys.* B (in press)
[29] Inogamov N A, Anisimov S I and Retfeld B 1999 *JETP* **88** 1143
[30] Inogamov N A, Zhakhovsky V V, Khokhlov V A, Demaske B J, Khishchenko K V and Oleynik I I 2014 *J. Phys.: Conf. Series* **500** 192023
[31] Yakovlev D G and Urpin V A 1980 *Sov. Astron. J.* **24** 303–10
[32] Fisher D, Fraenkel M, Henis Z, Moshe E and Eliezer S 2001 *Phys. Rev.* E **65** 016409
[33] Kresse G and Furthmuller J 1996 *Comp. Mater. Sci.* **6** 15
[34] Petrov Yu V and Inogamov N A 2013 *JETP Lett.* **98** 278
[35] Inogamov N A, Petrov Yu V, Khokhlov V A, Anisimov S I, Zhakhovskii V V, Ashitkov S I, Komarov P S, Agranat M B, Fortov V E, Migdal K P, Il'nitskii D K and Emirov Yu N 2014 *J. Opt. Tech.* **81** 233
[36] Hafner J 1987 *From Hamiltonians to Phase Diagrams* (Berlin, Heidelberg: Springer-Verlag)
[37] Grigoriev I S and Meilikhov E Z 1996 *Handbook of Physical Quantities* (CRC Press LLC)
[38] Rose J H, Smith J R, Guinea F and Ferrante J 1984 *Phys. Rev.* B **29** 2963
[39] Zhakhovskii V V, Inogamov N A, Petrov Yu V, Ashitkov S I and Nishihara K 2009 *Appl. Surf. Sci.* **255** 9592
[40] Powell R W, Ho C Y and Liley P E 1966 Thermal conductivity of selected materials *NSRDS-NBS 8 (Category 5—Thermodynamic and transport properties)*
[41] Mazevet S, Desjarlais M P, Collins L A, Kress J D and Magee N H 2005 *Phys. Rev.* E **71** 016409
[42] Matula R A 1979 *J. Phys. Chem. Ref. Data* **8** 1147
[43] Girifalco L A 2000 *Statistical Mechanics of Solids* (Oxford University Press)
[44] Norman G, Saitov I, Stegailov V and Zhilyaev P 2013 *Contrib. Plasma Phys.* **53** 300